Discover Applied Sciences

Research

Numerical investigation of scour around monopile foundation of offshore wind farm

Ebenezer Otoo[1] · Richard Asumadu[2,3] · Gideon Kwabena Boadi[1] · Jisheng Zhang[1] · Solomon Boadu[1] · Precious Mattah[2]

Received: 19 July 2023 / Accepted: 20 November 2023
Published online: 20 January 2024

Abstract
Local scour at the foot of monopile foundations is a major threat to the stability of offshore wind farms. This study presents a 3D numerical model to investigate the local scour around monopile foundations considering the influence of both flow velocity and particle size. The Reynolds-Averaged Navier–Stokes (RANS) equations with the Renormalization Group (RNG) k-epsilon ($k-\varepsilon$) turbulence model were coupled with a sediment transport model to simulate the flow-sediment interaction process. The results reveal that the maximum scour depth and the extent of the scour footprint increase with flow velocity and decrease with particle size. The scour rate is higher for finer sediments than for coarser sediments. The scour depth and footprint reach a plateau when the particle size is larger than a certain critical value. The critical particle size increases with the increase of flow velocity.

Article Highlights

- How scour depth formation is dependent on the sediment size and flow velocity.
- The increase and decrease in flow velocity increased the shear stress applied to the bed and thereby affecting scouring.
- A change in the period in all scenarios has a significant effect on scour depth.

Keywords Scour · Monopile · Offshore wind farm · Pile foundations · Sediment transport

1 Introduction

The global scale of offshore wind farms is escalating rapidly and vast wind offshore wind resources are being explored and exploited. For coastal engineers, the major challenge associated with offshore wind farms is to do with sediment and its dynamics. Unlike foundations placed on land, the foundations of offshore wind farms are exposed to harsh environmental conditions characterized by the marine environment, and the structure also must be stable on a continuously moving seabed [1, 2].

✉ Richard Asumadu, asumadur@yahoo.com | [1]College of Harbour, Coastal and Offshore Engineering, Hohai University, Nanjing 210098, China. [2]ACECoR, Centre for Coastal Management, University of Cape Coast, 00233 Cape Coast, Ghana. [3]Division for Coastal Engineering, Ghana Hydrological Authority, MB 501, Accra, Ghana.

Despite these challenges, the monopile foundation is the most popular concept of foundation for Offshore Wind Turbines (OWTs) due to its advantages such as its simplicity, prone and sensitivity to scour, applicability in soft and stiff soil, and convenience to construct [3, 4]. However, placing a structure in the marine environment causes gradients in the flow pattern and results in the removal of sediment near the foundation, preferably referred to as scour which threatens the stability of the foundation and structure [5–10].

The changes in flow pattern by the monopile foundation results in flow contraction, horseshoe vortex formation in front of the structure, lee-wake vortices behind the structure (with or without vortex shedding), reflection and diffraction of waves, wave breaking, turbulence generation, and pressure differentials in the soil leading to liquefaction [5, 11–16].

The physical modeling of seabed scour is challenged with scaling effects. Scaling problems faced in mobile bed studies of scouring was highlighted by [9], indicating the various parameters with which peculiar challenges may be faced including morphological features, bed-structure response, etc.

On the basis that numerical modeling can be used to solve complex boundary limitations in physical modeling, Sim and Choi [17] used a Flow 3D, Computational Fluid Dynamics (CFD) model, to investigate this challenge. They extended the boundary condition to an indefinite length and examined the free span development under the indefinite boundary condition. The results were in qualitative agreement with the laboratory results; however, the numerical model further revealed that the propagation of scour holes does not cease but continues to develop although at a slow and constant speed.

Thus, predicting localized pressure scour requires not only traditional laboratory experiments but needed also some numerical simulations, which are beyond the reach of physical modeling. Thus, the various advantages and ease of work associated with numerical models have led to their increase in many engineering applications in recent times [18, 19]

Therefore, numerical studies of local scour have gained roots with the rapid development of CFD [20]. The use of Flow3D software in simulating the flow field and sediment transport in modeling scouring considering the sand-sliding mechanism and bed slope effect has also been applied [15, 21].

Recently, there is the inclusion of the free surface effect in the flow model and scour around a circular pile [21–23], local scour around bridge piers [24, 25] and backfilling process around a vertical pile [26, 27]. The value of the stiffness of a foundation depends on the properties of the soil, hydrodynamic conditions, dimensions of the foundation, and the depth of the bedrock [28]. In this regard, it is prudent to combine the hydrodynamic conditions and the soil conditions to make a good assessment in understanding how mobile the bed material is [6, 29].

Therefore, in this study, a 3D integrated numerical model is developed using Flow3D software to investigate the phenomenon of sediment transport (Local Scour) around an offshore wind farm monopile foundation; particularly taking into consideration the effect of flow velocity and particle size on the changes in scour depth and extent. In other words, the paper aims to study how scour around a monopile foundation is affected by flow velocity and particle size. This is important because it can help engineers to design more stable and reliable offshore wind farms.

2 Theoretical model

In this section, the governing equations and boundary conditions used to develop the 3D numerical model in Flow3D are presented. The free surface is usually handled by the Volume of Fluid (VOF) technique, which was pioneered by Hirt and Nicholas [30]. The model addresses all the physics surrounding the problem or phenomenon of scouring, making it possible to fully understand scouring.

2.1 Momentum equation

The following three equations (RANS equations) are used to describe the incompressible viscous fluid motion by Yakhot and Orszag [31]. The equations of motion for the fluid velocity components (u, v, and w) with some additional terms in the three-coordinate *x*-, *y*-, and *z* directions are as follows:

$$\begin{aligned}
&\frac{\partial u}{\partial t}+\frac{1}{V_F}(uA_x\frac{\partial u}{\partial x}+vA_y\frac{\partial u}{\partial y}+wA_z\frac{\partial u}{\partial z})=-\frac{1}{\rho}\frac{\partial p}{\partial x}+G_x+f_x\\
&\frac{\partial v}{\partial t}+\frac{1}{V_F}(uA_x\frac{\partial v}{\partial x}+vA_y\frac{\partial v}{\partial y}+wA_z\frac{\partial v}{\partial z})=-\frac{1}{\rho}\frac{\partial p}{\partial y}+G_y+f_y\\
&\frac{\partial w}{\partial t}+\frac{1}{V_F}(uA_x\frac{\partial w}{\partial x}+vA_y\frac{\partial w}{\partial y}+wA_z\frac{\partial w}{\partial z})=-\frac{1}{\rho}\frac{\partial p}{\partial y}+G_z+f_z
\end{aligned} \tag{1}$$

where *xi* is the Cartesian coordinate, *Ai* is the area fraction, V_F is the volume fraction, u_i is the velocity, ρ is the fluid density, *p* is the average hydrodynamic pressure, *Gi* is the body acceleration, *fi* is the viscous acceleration (*i* = *x, y, z*).

2.2 Viscous accelerations model

The viscous accelerations are written as:

$$\begin{aligned}
\rho V_F f_x&=-\left[\frac{\partial}{\partial x}(A_x\tau_{xx})+\frac{\partial}{\partial y}(A_y\tau_{yx})+\frac{\partial}{\partial z}(A_Z\tau_{zx})\right]\\
\rho V_F f_y&=-\left[\frac{\partial}{\partial x}(A_x\tau_{xy})+\frac{\partial}{\partial y}(A_y\tau_{yy})+\frac{\partial}{\partial z}(A_Z\tau_{zy})\right]\\
\rho V_F f_z&=-\left[\frac{\partial}{\partial x}(A_x\tau_{xz})+\frac{\partial}{\partial y}(A_y\tau_{yz})+\frac{\partial}{\partial z}(A_Z\tau_{zz})\right]
\end{aligned} \tag{2}$$

in which *τij* is the shear stresses (*i, j* = *x, y, z*):

$$\begin{aligned}
\tau_{xx}&=-2\mu\left[\frac{\partial u}{\partial x}-\frac{1}{3}(\frac{\partial u}{\partial x}+\frac{\partial v}{\partial y}+\frac{\partial w}{\partial z})\right] & \tau_{xy}&=\tau_{yx}=-\mu\left(\frac{\partial u}{\partial x}+\frac{\partial v}{\partial y}\right)\\
\tau_{yy}&=-2\mu\left[\frac{\partial v}{\partial y}-\frac{1}{3}(\frac{\partial u}{\partial x}+\frac{\partial v}{\partial y}+\frac{\partial w}{\partial z})\right] & \tau_{xz}&=\tau_{zx}=-\mu\left(\frac{\partial u}{\partial x}+\frac{\partial w}{\partial z}\right)\\
\tau_{zz}&=-2\mu\left[\frac{\partial v}{\partial z}-\frac{1}{3}(\frac{\partial u}{\partial x}+\frac{\partial v}{\partial y}+\frac{\partial w}{\partial z})\right] & \tau_{zy}&=\tau_{yz}=-\mu\left(\frac{\partial w}{\partial z}+\frac{\partial v}{\partial y}\right)
\end{aligned} \tag{3}$$

where μ is the dynamic viscosity.

2.3 Turbulent transport model

K-ε model has proven to provide approximations to many types of flows [32]. In the RNG model, the empirical constants of the equation in the *k-ε* model were explicitly derived. The *k-ε* model consists of two transport equations for the turbulent kinetic energy k^T and its dissipation ε_T, a widely used and sophisticated model [33]. An additional transport equation is solved for the turbulent dissipation, ε_T:

$$\frac{\partial \varepsilon_T}{\partial t}+\frac{1}{V_F}\left\{uA_x\frac{\partial \varepsilon_T}{\partial x}+vA_yR\frac{\partial \varepsilon_T}{\partial y}wA_z\frac{\partial \varepsilon_T}{\partial z}\right\}=\frac{CDIS1\cdot\varepsilon_T}{k_T}\left(P_T+CDIS3\cdot G_T\right)+Diff_\varepsilon-CDIS2\frac{\varepsilon_T^2}{k_T} \tag{4}$$

where *CDIS1*, *CDIS2*, and *CDIS3* are all dimensionless user-adjustable parameters and have defaults of 1.44, 1.92, and 0.2 respectively for the *k-ε* model.

In the transport equation for k_T, the convection and diffusion of turbulent kinetic energy, diffusion, and dissipation due to viscous losses within the turbulent eddies, and the production of turbulent kinetic energy due to shearing and buoyancy effects were all included where buoyancy only occurs if there is a non-uniformity in the flow density and the effects of gravity and non-inertial accelerations are inclusive. The transport equation then is represented by:

$$\frac{\partial k_T}{\partial t}+\frac{1}{V_F}\left\{uA_x\frac{\partial k_T}{\partial x}+vA_y\frac{\partial k_T}{\partial y}wA_z\frac{\partial k_T}{\partial z}\right\}=P_T+G_T+Diff_{k_T}-\varepsilon_T \tag{5}$$

where V_F, A_x, A_y, and A_z are Flow3D's FAVOR™ functions, P_T is the turbulent kinetic energy production.

2.4 Sediment scour model

In this study, the mechanisms of entrainment and deposition are treated as two opposing signs of progress that occur at the same time, which are combined to determine the net rate of the exchange between the packed sediment and the suspended sediment. Therefore, the entrainment lift velocity of sediment was computed according to Mastbergen and Van Den Berg [34]:

$$u_{lift,i} = \alpha_i n_s d_*^{0.3} \left(\theta_i - \theta_{cr,i}\right)^{1.5} \sqrt{\frac{\|g\| d_i (\rho i - \rho f)}{\rho f}} \tag{6}$$

where α_i is the entrainment parameter, the recommended value is 0.018, n_s is the outward pointing normal to the packed bed interface, d_* is the dimensionless diameter of the sediment, θ_i is the local shields parameter which is calculated based on the local bed shear stress, $\theta_{cr,i}$ is the critical shields parameter, g is the magnitude of the acceleration of gravity, d_i is the diameter, ρi is the density of the sediment species, and ρf is the fluid density.

The settling velocity of the sediment was computed according to Soulsby [35]

$$u_{settling,i} = \frac{v_f}{d_i}\left[\left(10.36^2 + 1.049 d_*^3\right)^{0.5} - 10.36\right] \tag{7}$$

where v_f is the kinematic viscosity of the fluid.

This study also used the model of [35, 36] to predict the volumetric flow rate of sediment per unit width over the surface of the packed bed; expressed as:

$$\phi_i = \beta_i \left(\theta_i - \theta''_{cr,i}\right)^{1.5} \tag{8}$$

where θ_i is the dimensionless local bed shear and Φ_i is the dimensionless bed-load transport rate.

The suspended sediment concentration is calculated by solving its transport equation:

$$\frac{\partial C_{s,i}}{\partial t} + \nabla.\left(u_{s,i} C_{s,i}\right) = \nabla.\nabla\left(D_f C_{s,i}\right) \tag{9}$$

where $C_{s,\,i}$ is the suspended sediment mass concentration of species i, which is defined as the sediment mass per volume of the fluid-sediment mixture, $u_{s,i}$ is the sediment velocity of species i, and D_f is the diffusivity.

Each sediment species in suspension moves at a velocity caused by the different inertia and drag forces for each grain with different mass densities and sizes. With the assumptions that there are no strong interactions between each grain and that the velocity difference between the suspended grains and the fluid-sediment mixture is mainly the setting velocity of the grains, the sediment velocity of species i was calculated as;

$$u_{s,i} = \overline{u} + u_{settling,i} C_{s,i} \tag{10}$$

where u denotes the velocity of the fluid-sediment mixture, which was obtained by solving the continuity and Navier–Stokes equations closed with the *RNG k-ε* turbulence model and $c_{s,i}$ is the suspended sediment volume concentration.

2.5 Model setup

The numerical model for the fluid-seabed—pile was set up in a rectangular domain of 2 m × 1 m x 60 cm (long x wide x deep) respectively with packed sediment consisting of uniform granular sediment with a median diameter d_{50} of 1.63 mm as shown in Fig. 1. A 10 cm-diameter pile with a height of 60 cm was situated 1.4 m away from the inlet of the domain and at the exact center in the *y*-direction, 0.5 m. This pile had an embedded length of 30 cm with the remaining 30 cm above the bed level. The domain was filled with sediment at a bed thickness of 0.3 m, and fluid was allowed into the domain from the X_{min} at a height of 7.5 cm.

Figure 2 shows the mesh grid for the model. The domain had uniform mesh cells of size 0.2 cm and 25.5 cm,75.0 cm.

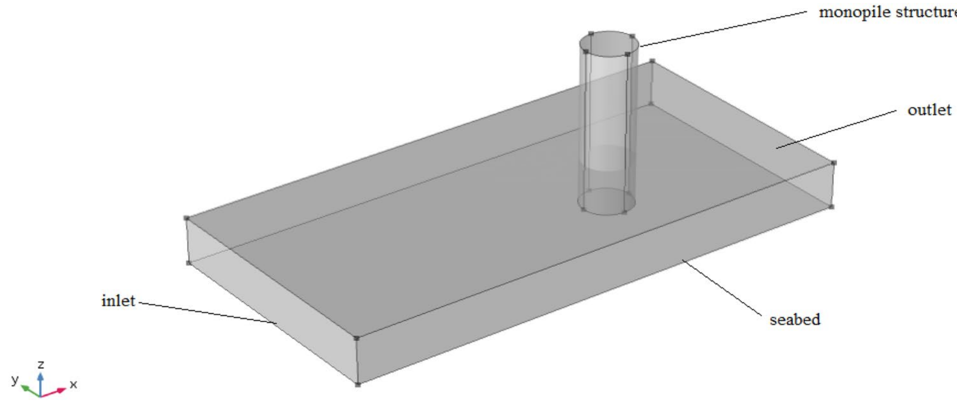

Fig. 1 The computation domain used for the simulation

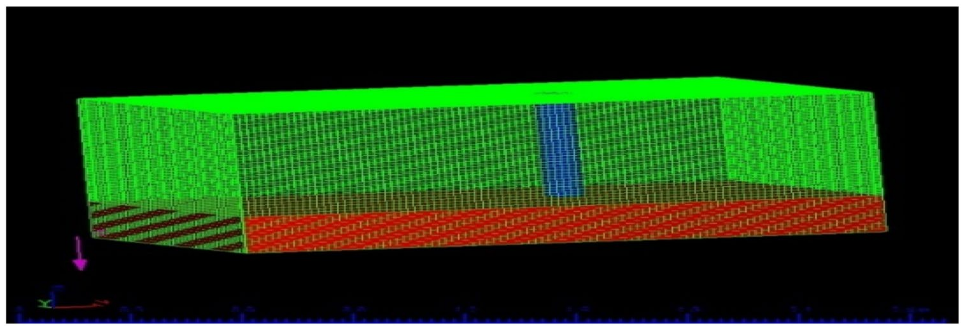

Fig. 2 Domain setup in Flow-3D model

2.6 Add boundary conditions

2.6.1 Boundary conditions

Appropriate boundary conditions are very important at the external boundaries and internal interface and are required to solve the Navier–Stokes governing equations.

1. Advective and diffusive fluxes are set to zero at the rigid walls where the fractional open areas vanish.
2. Tangential stresses are as well set to zero at the free surfaces due to the vanishing velocity derivatives that are across the surface. At the inlet boundary, a defined fluid velocity is set and introduced into the domain and the fluid is allowed to move out of the domain without returning to the system with an outflow boundary condition set to the outlet, X_{max}.
3. The Outflow boundary is adopted at the outflow boundary, which is a radiation boundary condition; to avoid the reflection of flow and overcome the limitation of physical dimensions. Therefore, it was imagined that there is a mathematical continuation of the flow beyond the end of the computed region. Thus, there is no sponge layer or damper used in the domain.
4. At the Z_{max} boundary, the specified pressure is set at zero with a fluid fraction of zero as fluid is expected not to exit that boundary. The pile surfaces are treated as a no-slip boundary, and the turbulence properties are estimated from the law of the Wall boundary condition.

3 Model validation

In this section to ascertain the accuracy of the simulation results, the present numerical model was validated against a set of published experimental and other numerical test results.

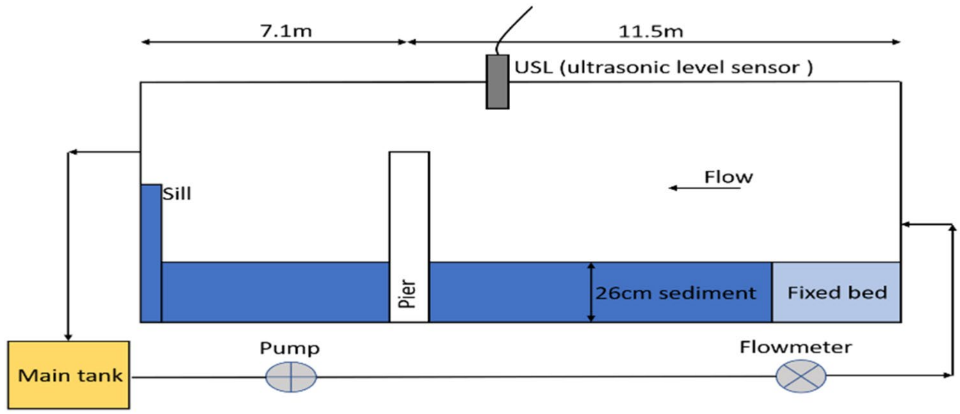

Fig. 3 Setup of experimental laboratory work conducted by Aksoy and Eski [37]

Table 1 Model validation comparison results

Results	*D* (cm)	d_S (cm)	L_s (cm)
Aksoy and Eski	11	4.7	7.5
Present work	11	4.7	7.0

D is pile diameter, d_s is maximum scour depth and L_s is the scour extent in the *x*-direction

3.1 Comparison with Aksoy and Eski's [37] physical experiment

The model was validated with the same experimental setup by Aksoy and Eski [37]as shown in Fig. 3. In the experiment by Aksoy and Eski, four piles of different diameters were used for the investigation at different discharge rates. One out of the four piers was selected for the model validation; and in this case, the 11 cm diameter pile was based on a lot of decision-influencing factors such as the influence of the blockage effect, the domain size, amongst others, and not by random selection or some convenient sampling procedure.

For the two investigations, the maximum scour depth measured, $d_s = 4.7$ cm. It can be seen that the maximum scour depth measure for the two different models are the same and equal however with a slight difference in the measured extent of the scour with the experimental investigation of [37] yielding an extent of 7.5 cm whereas the present numerical simulation produced 7.0 cm. Hence, the difference in the extent was 0.5 cm as presented in Table 1.

3.2 Comparison with Wei [38] and Zhang [10] numerical model

The present numerical model is compared with results from [38]. It was found that the velocities in the x-direction at the piers are low and the pattern is closely similar to that observed by [38] with a slight difference in the magnitude of velocities; which can be attributed to factors including but not limited to fluid depth, bed thickness to water column ratio, and distance traveled by the fluid before it comes into contact with the structure.

Furthermore, similar to [10] who validated their model numerically using the parameters of [38], the results from this study are in good agreement with [38] but with some differences in scour depth as shown in Fig. 4. Nevertheless, the full principles associated with scour (such as; deposition and erosion profiles, velocity profiles, etc.) were observed in all three cases. The scouring depth produced by this study was 0.87 m, which is 0.58D. From the results of [38] a scouring depth of 0.79 m which is 0.52D was produced while that of [10] produced a scour depth of 0.74 m which is 0.49*D*. The differences in the scour depths may be said to be a result of the differences in some of the model settings such as the total number of cells, cell size, uniformity, and/or un-uniformity of cells among others. Nonetheless, the results are in good agreement with a micro range of margins. Thus, affirming the reliability of the simulation results from this study to achieve the desired objectives.

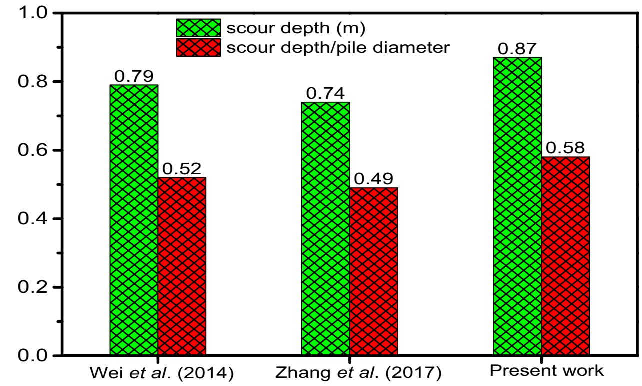

Fig. 4 Scour depth comparison with [10, 38]

4 Results

This paper aims to develop a 3D numerical model to investigate scouring around monopile foundations. In this section, A total of four simulations were undertaken to appreciate the changes in scour depth and extent (i.e., the entire footprint of the scour) with respect to all other parameters except for fluid flow velocity and sediment particle size which were adjusted. The numerical model is set up in a domain as presented in Fig. 1. Table 2 tabulates the input parameter for the four scenarios.

4.1 Yardstick simulation

After 360 s of simulation time, results produced showed the progressiveness of the transport of sediment and excavation of sediment at the foot of the foundation which was a result of the downflow of the fluid at the stagnation point and the vortices created as presented in Fig. 5. Sediment deposition was observed at the lee-side of the pile as flow velocity in that region reduced significantly thereby making the bed shear threshold not being met or overcome by the stress applied there by the fluid.

As shown in Fig. 6, there was a reduction in the bed level by 6.8 cm in front of the pile foundation, with an increase in the bed elevation behind the pile foundation through sediment deposition, which was recorded at some 1.57 cm above the initial bed level. The maximum scouring depth of 9 cm which is 0.9*D* was first recorded after 142 s of simulation time at the 191 data point when the scour depth was at equilibrium with the extent of scour at 19.37 cm*32.78 cm (x*y directions). Upon the final simulation time of 360 s, the maximum scour depth had stabilized but the scour extent had increased to some 28.31 cm*37.25 cm (*x*y* directions).

Although the bed deforms generally (general scour), upon the introduction of the fluid into the domain, it was observed that at the immediate foot of the foundation, there is the creation of a pit (local scour) which results from the obstruction of the flow by the foundation. The general bed level changes are attributed to the dynamics with regard to the hydrodynamics. A 3D representation of the bed transformation in time with respect to fluid flow and sediment response in space and time, *x* is shown in Fig. 7.

Table 2 Simulations and their parameters

Simulation	Parameter (s)						Domain		
	d_{50} (mm)	Fluid Velocity (m/s)	Fluid Depth (cm)	Pile diameter, *D* (cm)	Period (s)	Pile Height (cm)	X (m)	Y (m)	Z (m)
Yardstick	0.75	0.64	7.5	10	360	60	2	1	0.6
Increased velocity	0.75	0.74	7.5	10	360	60	2	1	0.6
Reduced velocity	0.75	0.54	7.5	10	360	60	2	1	0.6
Coarse sediment	1.55	0.64	7.5	10	360	60	2	1	0.6

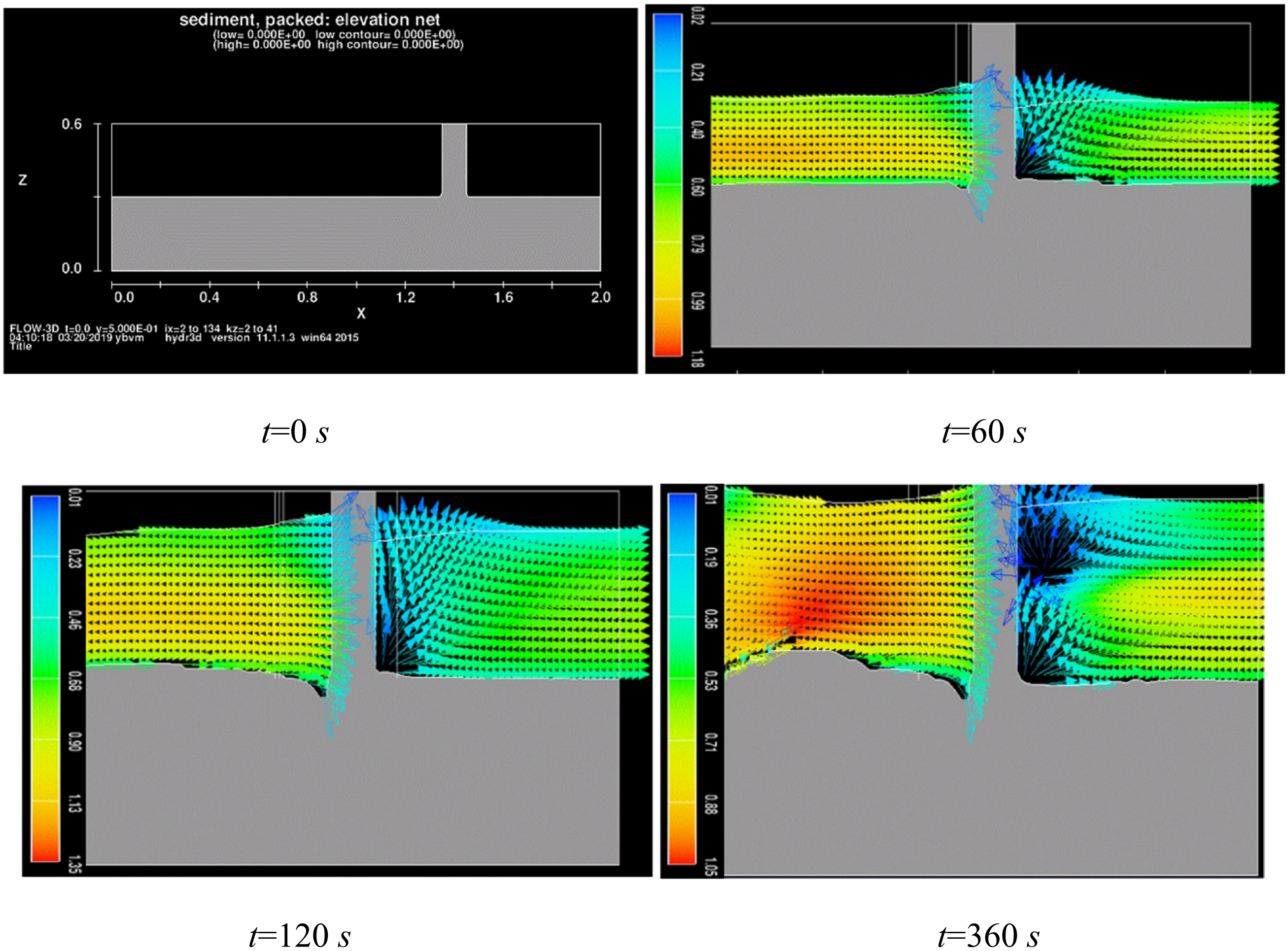

Fig. 5 Cross-sectional illustration of bed elevation changes around the pile in the *x*–*z* plane

4.2 Effect of coarse sediment

Particle diameter is an important factor that affects scouring. The larger the particle diameter, the more resistant the sediment is to erosion. This is because larger particles have more inertia and are therefore more difficult to dislodge.

To appreciate the changes that the physical parameters impose on the maximum scour depth, a simulation was run to comprehend the changes caused by an adjustment of the particle size (i.e., coarser (1.55 mm) than in the Yardstick scenario) as shown in Figs. 8 and 9. The equilibrium scour was first recorded after 150 s of the simulation time and thus the 201 data recording point. The equilibrium scour was first recorded after 150 s of simulation time and thus the 201 data recording point. The scour extent at the time the scour depth was in equilibrium was 19.37 cm*25.33 cm (*x***y* directions). After the final simulation time of 360 s, the extent of scouring had increased to 20.86 cm*29.80 cm (*x***y* directions).

Compared to the yardstick simulation, the time for equilibrium scour depth to be met was elongated because the bed-shearing threshold had increased. For the same depth of sediment excavation to be achieved, the turbulence effect had to be persistent on the bed for quite a while then in the case of the yardstick simulation. Thus, the coarser the particle size, the greater the critical shear stress or bed shearing threshold. Therefore, the intensity of the disturbance caused to the bed was resistible in a higher value than in the case of the first scenario when the particles were fine. Hence, the susceptibility of the bed to scouring was alleviated and thus accounted for the increase in time taken for the fluid to cause the same effect (i.e., equilibrium scour and maximum scour depth).

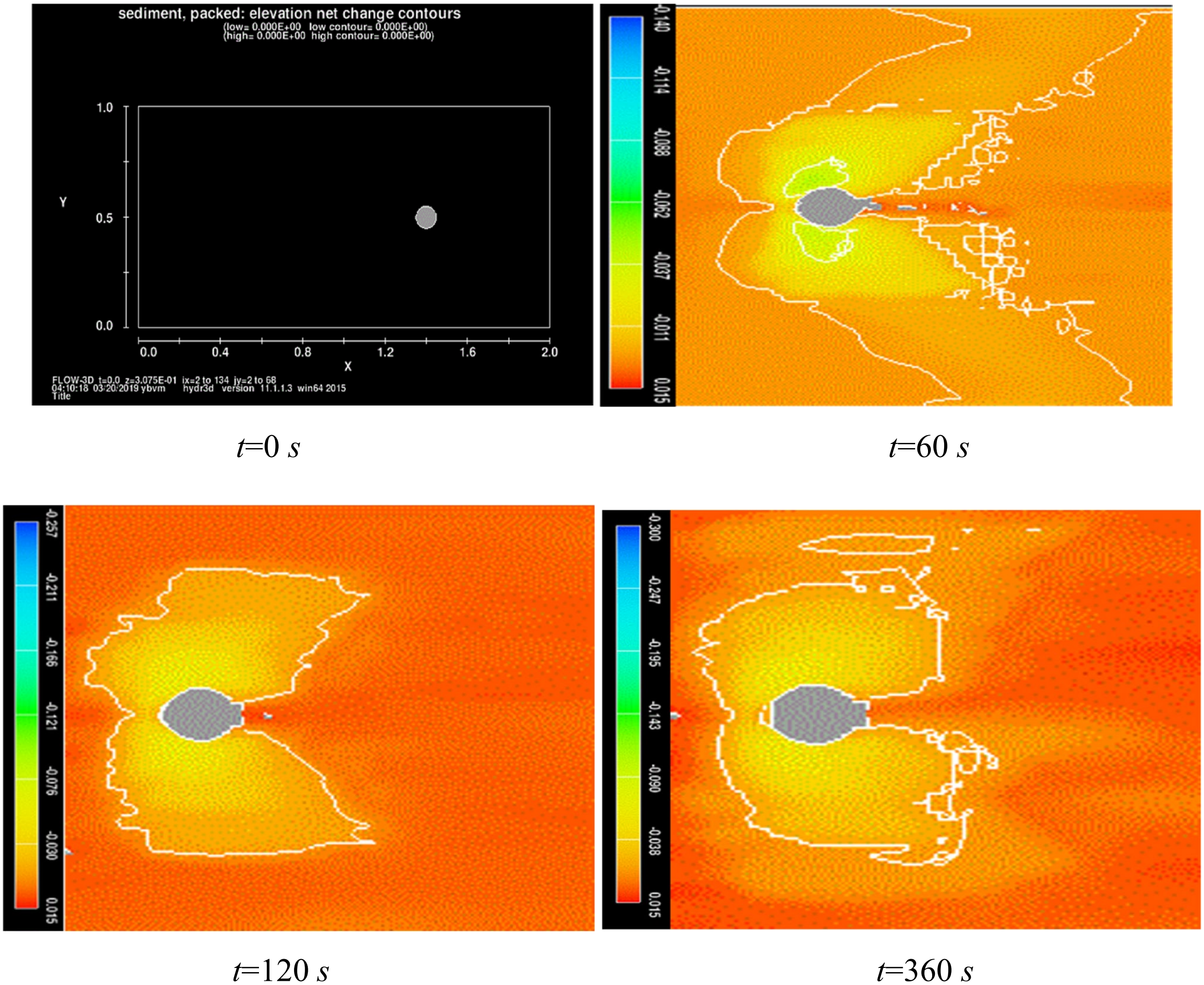

Fig. 6 Scour formation pattern around the pile in the *x*–*y* plane

4.3 Effect of increased flow velocity

Flow velocity is one of the most important factors that affect scouring. The higher the flow velocity, the greater the shear stress on the seabed, which can lead to more sediment being eroded and transported. The shear stress is proportional to the square of the flow velocity. This means that doubling the flow velocity will quadruple the shear stress. Therefore, scouring is a non-linear process, and it can increase very rapidly with increasing flow velocity.

As the flow velocity was increased as shown in Figs. 10 and 11, the maximum scour depth occurred quite earlier at some 81 *s* of simulation time at the 110th data point with a recorded scour extent of 23.84 cm*34.27 cm (*x***y* directions). The depth of scouring remained at equilibrium till the end of the run-time but the extent and general footprint of the scour kept changing and at the final simulation time of 360 *s*, the scour extent was 26.82 cm*28.31 cm (*x***y* directions).

It can be inferred that the increase in flow velocity increased the shear stress applied to the bed, leading to the removal of sediment at a shorter time compared to the yardstick simulation making the bed more susceptible to scour. Thus, the critical shear stress of the bed is exceeded by the stress imposed on it by the disturbance caused by the flow-induced vortex with high intensities and suspension capacities.

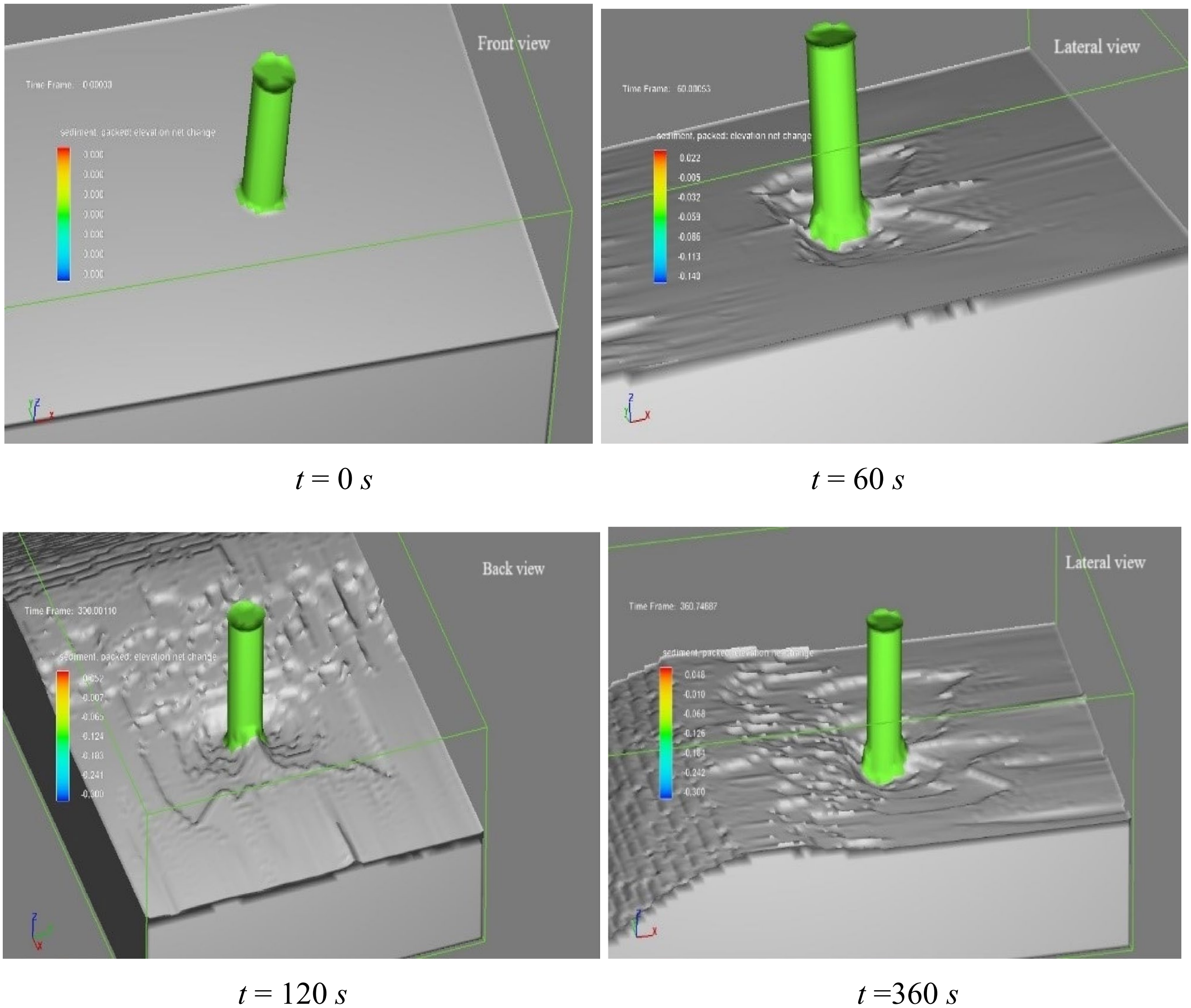

Fig. 7 3D representation of bed deformation and local scour formation

4.4 Effect of reducing flow velocity

Since scouring is a non-linear process, and it can decreases very rapidly with decreasing flow velocity. The flow velocity was reduced to understand its impact on scour footprint, thus the extent and the maximum scour depth. As shown in Figs. 12 and 13, a decrease in flow velocity reduced the scour extent. A maximum scour depth of 9 cm was first recorded after 281 *s* of simulation time at the 377th data point when the scour depth was at equilibrium with the extent of scour at 17.88 cm*32.78 cm (*x*y* directions).

Upon the final simulation time of 360 *s*, the maximum scour depth had stabilized but the scour extent had increased to some 22.35 cm*34.27 cm (*x*y* directions). In this case, even though the bed was susceptible to scouring, the mechanism that was to keep the sediment in suspension for further transportation away from their initial positions was not strong enough to move a large quantum of sediment. Thus, just a relatively smaller mass of sediment was relocated as the sediment particles were more resistant to the lift and drift mechanisms imposed on them.

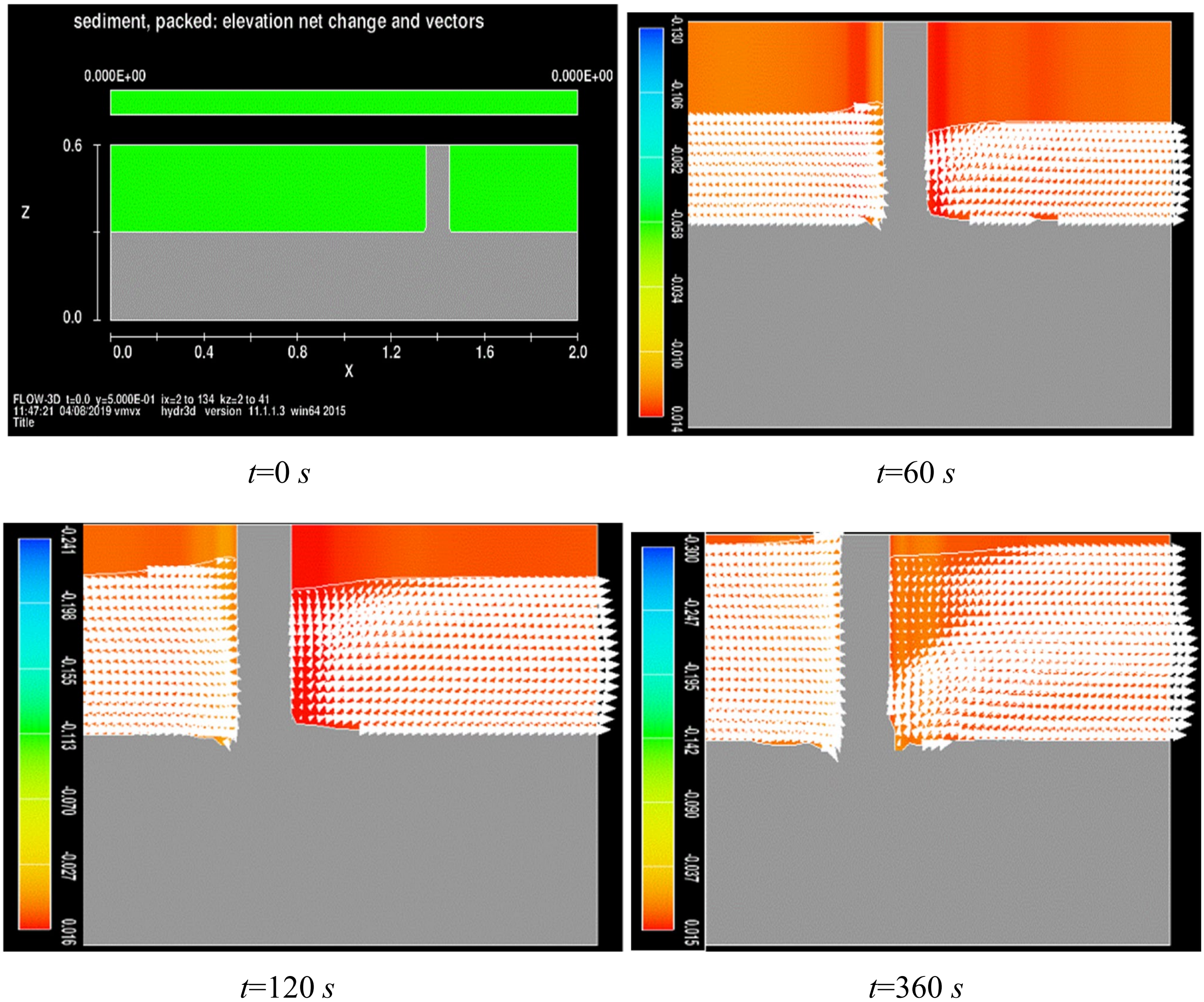

Fig. 8 Scour at the pile front and deposition behind the pile for the coarse seabed

5 Discussion

The emergence of scour around the monopiles is one of the main reasons for concern regarding the stability of monopiles. Which can weaken the foundation and make the monopile more likely to collapse. As a result, engineers and scientists are therefore interested in determining reliable methods of reducing and controlling local scour depth, in order to improve the safety of monopiles. Wave flowing around a monopile can cause the seabed to erode, creating a hole or depression called scour. This can happen because the water flows down and around the pile, creating vortices or swirls. The vortices can pick up and carry away sediment, leaving the seabed exposed. which can weaken the foundation of the monopile and make the monopile more likely to collapse. Both armoring devices and flow-altering methods are the two most effective techniques in reducing local scour for monopiles. The best approach will depend on the specific site conditions and severity of the scour problem.

This study aims to investigate how flow velocity and sand particle sizes affect the depth and size of scour holes. Scour holes are a common cause of monopile failure, and governments and agencies spend billions of dollars each year to repair damage caused by scour.

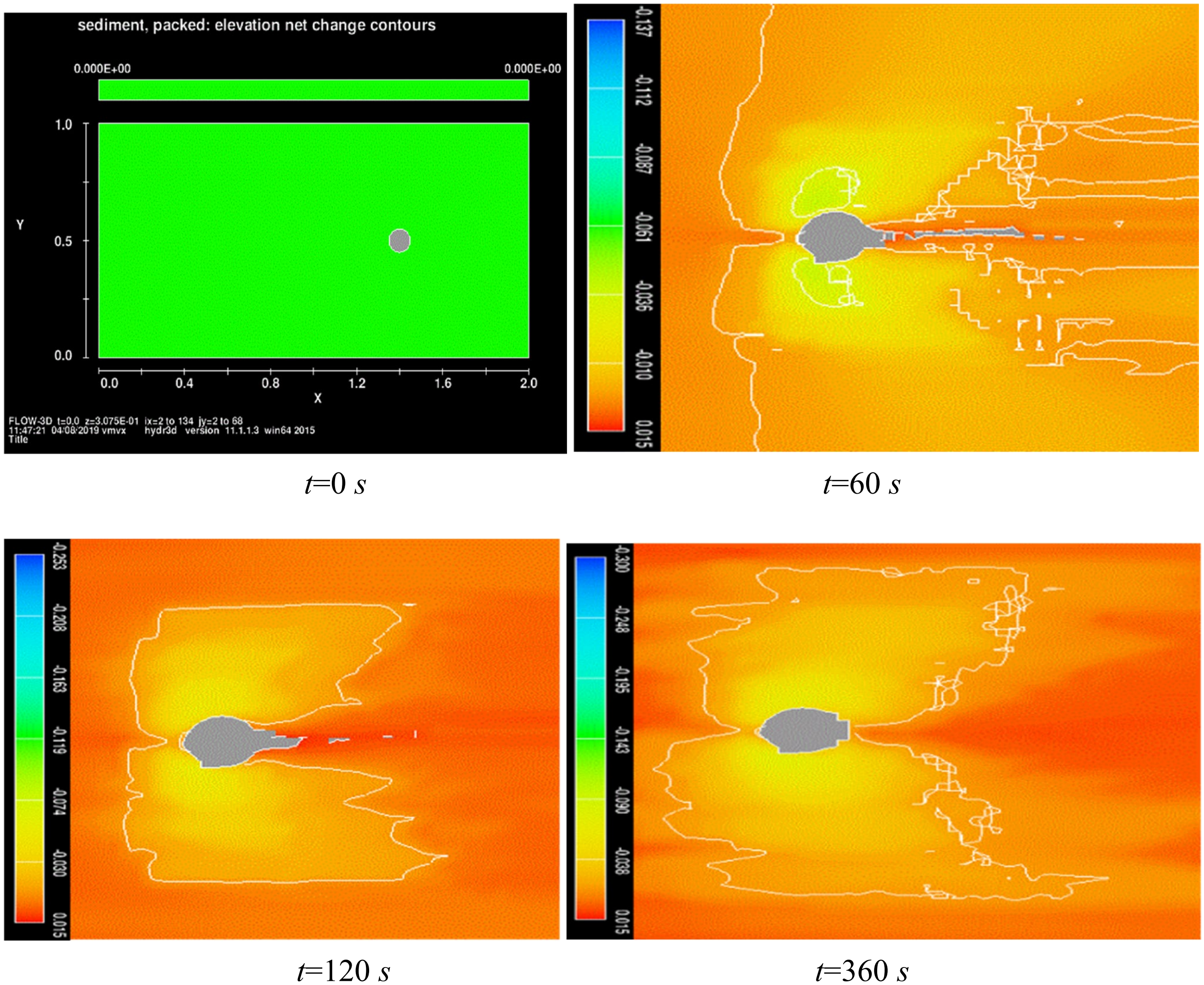

Fig. 9 Scour depth and extent for the coarse seabed

5.1 Comparison of results

Comparing the observation for the four simulations as presented in Fig. 14, it was realized that the maximum scour depth in all the scenarios was the same (at 9 cm) but at different times. Nevertheless, the scour extent and footprint did cover different zones, thus the dimensions of the extent of scouring were not equal, hence differed in each scenario.

5.2 Comparison of results with previous studies

After achieving the scour depths results as shown in Fig. 14 based on the equation, we compared our study to other research with similar hydraulic conditions. Accordingly, this present research work is compared with other previous numerical works such as [39, 40], all based on the RAN equation and k – ε turbulence model equations. It was concluded in all this research that the pile diameter plays a very significant role in local scouring. On the other hand flow velocity and particle size diameter greatly contribute to scour. This concludes that the shear stresses are proportional to the square of the flow velocity. This means that doubling the flow velocity will quadruple the shear stress. Therefore, scouring is a non-linear process, and it can increase very rapidly with increasing flow velocity.

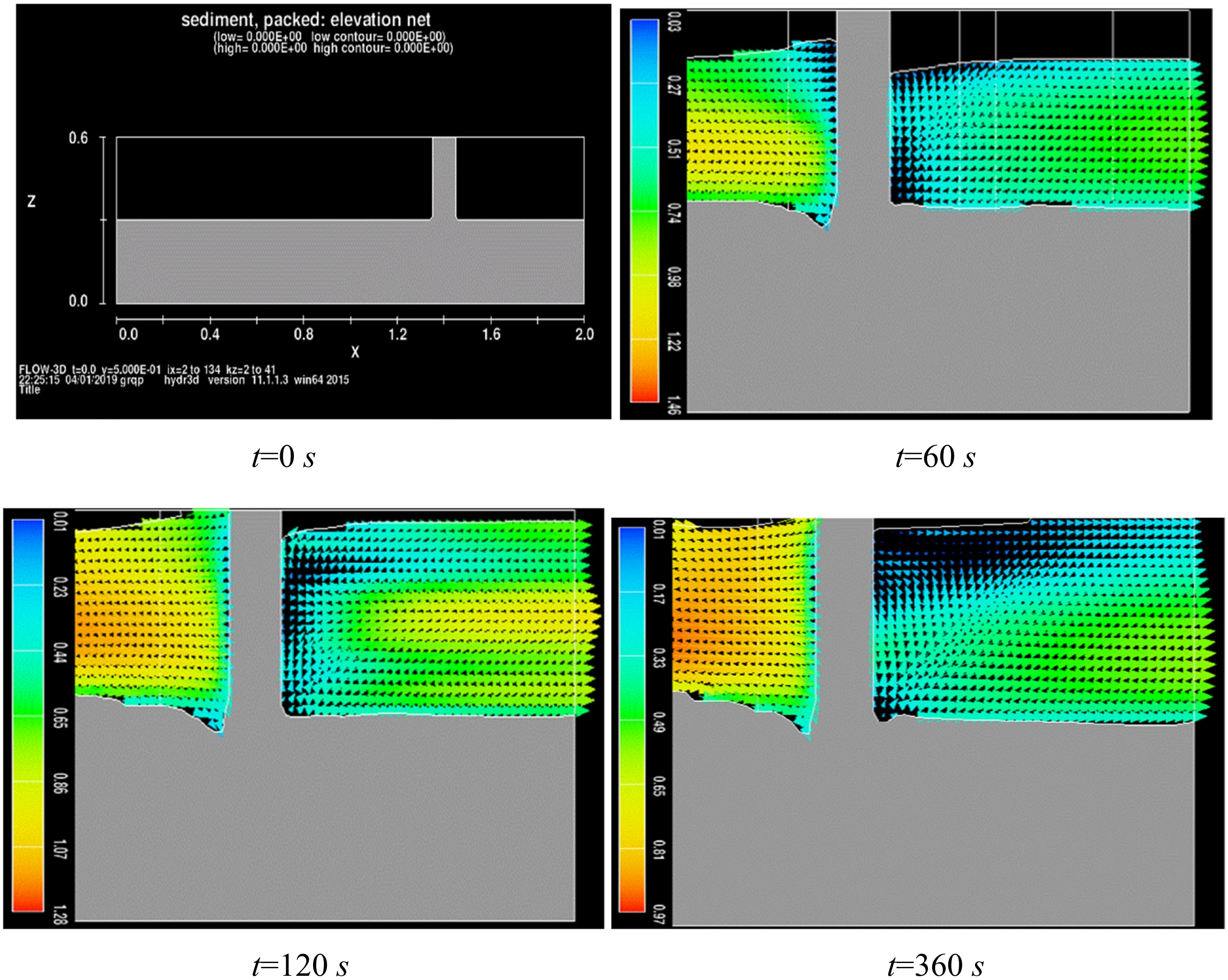

Fig. 10 Propagation of scour around the monopile

6 Conclusions

In this study, a 3D numerical model is developed using Flow3D software to investigate the role of flow velocity and particle size in the changes in scour depth and extent. The present model was verified with results from other studies and found to be in good agreement.

With the changes in sediment size and flow velocity, the formation of significant scour depth and extent was observed for all four simulations conducted. The time record for maximum and equilibrium scour depth formation was dependent on the sediment size and flow velocity. With a coarser sediment size, the time for equilibrium scour depth to occur was extended compared to the yardstick simulation because the bed-shearing threshold had increased. An increase in flow velocity increased the shear stress applied to the bed, leading to sediment removal at a than the yardstick simulation, making the bed more susceptible to scour. Even though scour was observed for decreased flow velocity, a relatively smaller mass of sediment was relocated as the sediment particles were more resistant to the lift and drift mechanisms imposed on them.

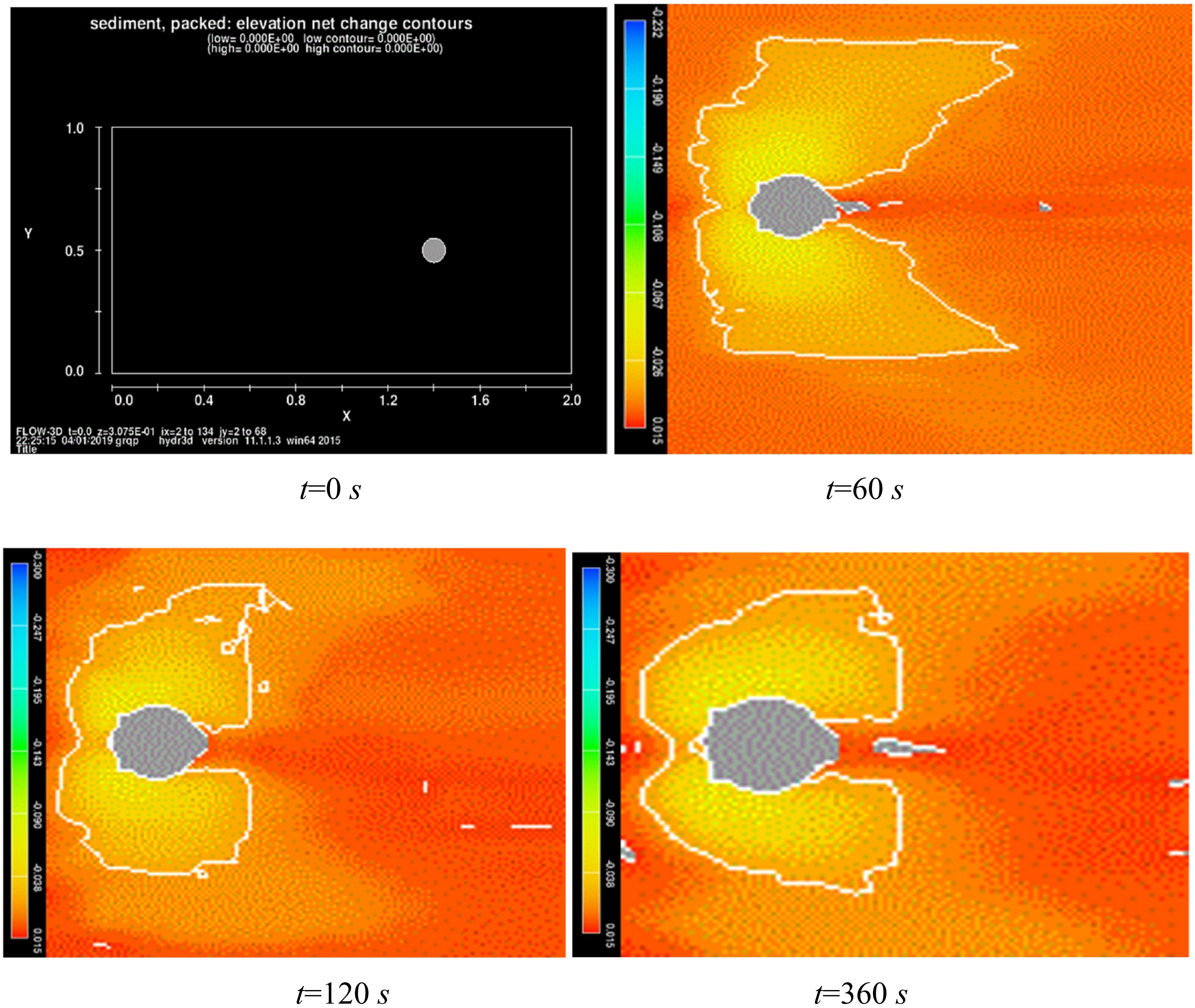

Fig. 11 Scour footprint at the foot of the foundation

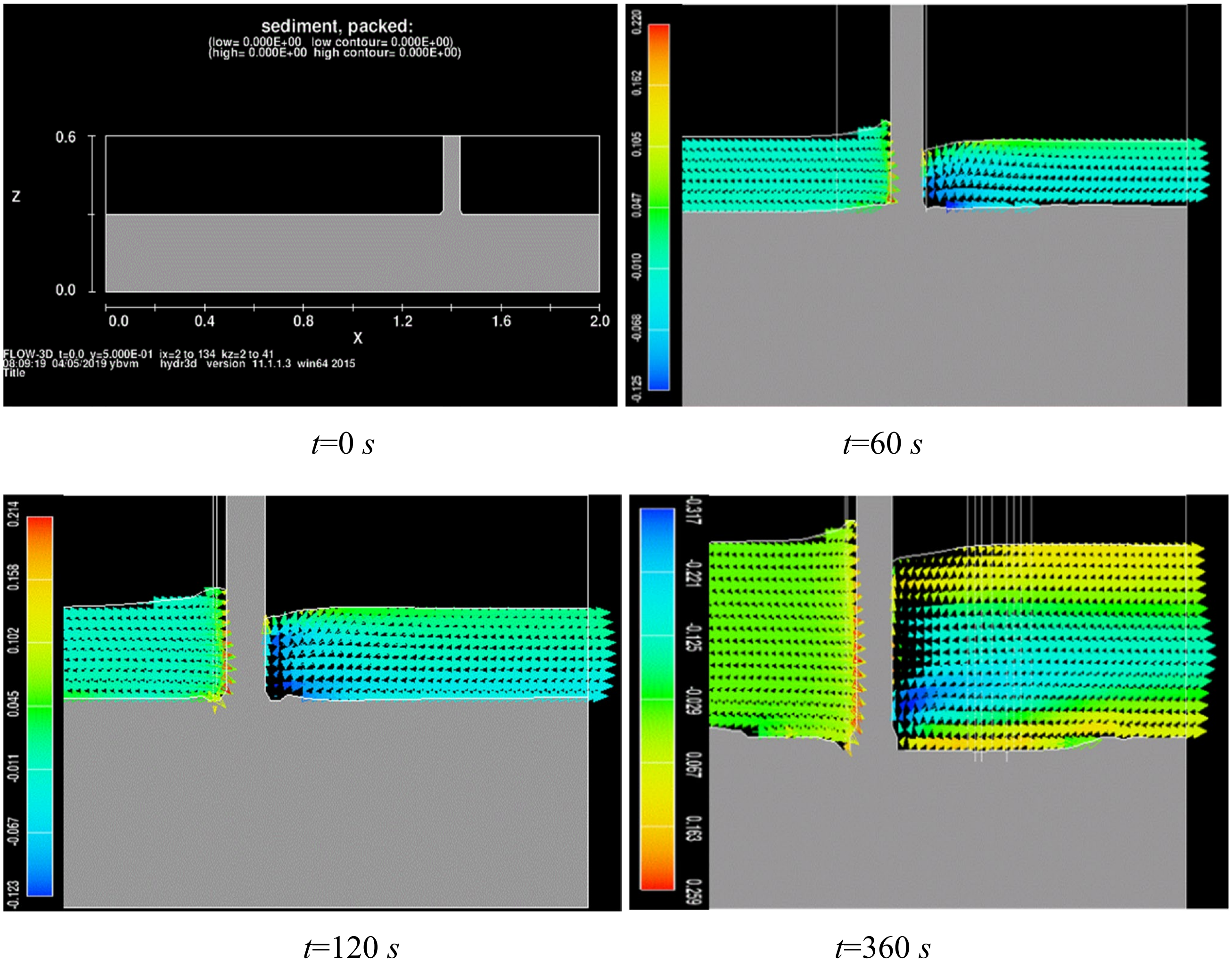

Fig. 12 Extent of scour development

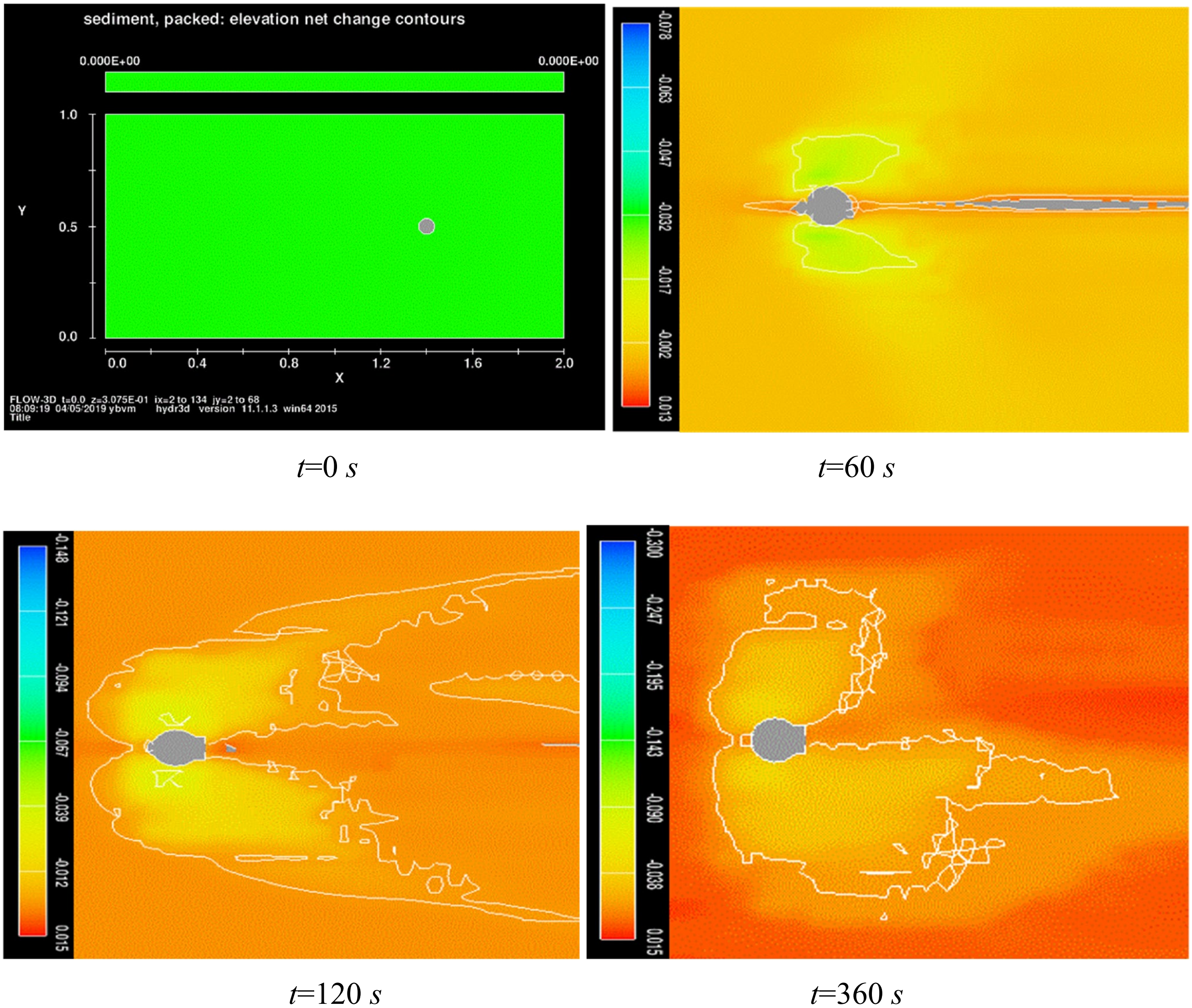

Fig. 13 Scour footprint at a reduced flow velocity

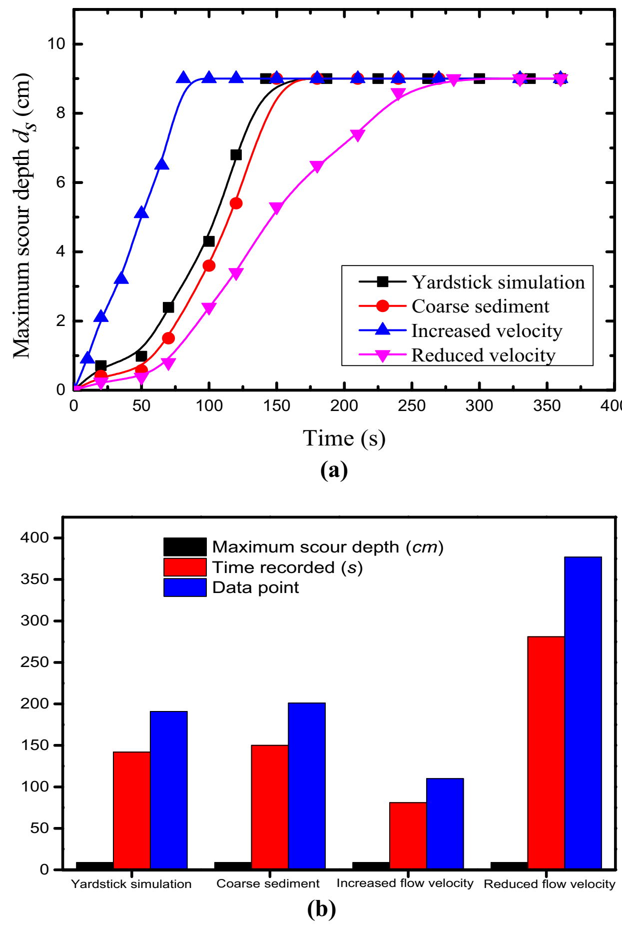

Fig. 14 Comparison of the results from the four simulations: (a) scour propagation; (b) duration for scouring equilibrium

Acknowledgements We are grateful to the University of Cape Coast and Hohai University for their help

Author contributions EO data collection and wrote part of the manuscript: RA conceptualized the idea and analysed the results while; GKB reviewed the manuscript. JZ reviewed and commented on the manuscript; SB commented on the manuscript; PM reviewed the final draft.

Funding No funding for this research.

Data availability All the data, and codes that support the findings of this study, including the flow3D models setup, are available from the corresponding author upon reasonable request.

Declarations

Competing interests The authors declare no competing interests.

References

1. Ye J, Wang G. Seismic dynamics of offshore breakwater on liquefiable seabed foundation. Soil Dyn Earthq Eng. 2015. https://doi.org/10.1016/j.soildyn.2015.02.003.
2. Zhang JS, Zhang C, Jeng DS. Three-dimensional model for wave-induced dynamic pore pressure around monopile foundation. AIP Conf Proc. 2012. https://doi.org/10.1063/1.4756441.

3. Hammar L, Andersson S, Rosenberg R (2010) Adapting offshore wind power foundations to local environment. Naturvårdsverket
4. Asumadu R, Zhang J, Zhao HY, Osei-Wusuansa H, Akoto AB. 3-Dimensional numerical study of wave-induced seabed response around three different types of wind turbine pile foundations. SN Appl Sci. 2019. https://doi.org/10.1007/s42452-019-1484-2.
5. Sutherland J, Whitehouse RJS (1998) Scale effects in the physical modelling of seabed scour
6. Whitehouse RJS (2004) Marine scour at large foundations
7. Jeng DS, Bateni SM, Lockett E (2005) Neural Network assessment for scour depth around bridge piers (No. R855)
8. Petrinia F, Li H, Bontempi F. Basis of design and numerical modeling of offshore wind turbines. Struct Eng Mech. 2010;36:599–624.
9. Whitehouse RJS, Sutherland J, Harris JM (2011) Evaluating scour at marine gravity foundations. Proc Inst Civ Eng Eng Thomas Telford Ltd, pp 143–157
10. Zhang Q, Zhou XL, Wang JH. Numerical investigation of local scour around three adjacent piles with different arrangements under current. Ocean Eng. 2017. https://doi.org/10.1016/j.oceaneng.2017.07.045.
11. Whitehouse RJS (2006) Scour at coastal structures
12. Melville B (2008) The physics of local scour at bridge piers. In: Fourth international conference on scour and erosion, pp 28–38
13. Sumer BM, Fredsøe J. Scour around pile in combined waves and current. J Hydraul Eng. 2001;127:403–11.
14. Harris JM, Whitehouse RJS, Sutherland J (2011) Marine scour and offshore wind: lessons learnt and future challenges. In: International conference on offshore mechanics and arctic engineering, pp 849–858
15. Centen I (2015) Predicting scour around offshore wind turbines using soft computing techniques
16. Sumer BM, Fredsøe J (2002) Time scale of scour around a large vertical cylinder in waves. In: ISOPE international ocean and polar engineering conference, p ISOPE-I
17. Sim YC, Choi S (2010) Three-dimensional scour at submarine pipelines under indefinite boundary conditions pipeline are performed in terms of flume tests . However , boundary conditions are restricted in
18. Chanel PG (2009) An evaluation of computational fluid dynamics for spillway modeling
19. Chanel PG, Doering JC. Assessment of spillway modeling using computational fluid dynamics. Can J Civ Eng. 2008;35:1481–5.
20. Boroomand MR, Salehi Neyshabouri SAA, Aghajanloo K. Numerical simulation of sediment transport and scouring by an offset jet. Can J Civ Eng. 2007;34:1267–75.
21. Roulund A, Sumer BM, Fredsøe J, Michelsen J. Numerical and experimental investigation of flow and scour around a circular pile. J Fluid Mech. 2005;534:351–401.
22. Ahmad N, Afzal S, Bihs H, Arntsen ØA (2015) Three-dimensional numerical modeling of local scour around a non-slender cylinder under varying wave conditions. 36th IAHR world Congress
23. Dutta D, Bihs H, Afzal MS. Computational fluid dynamics modelling of hydrodynamic characteristics of oscillatory flow past a square cylinder using the level set method. Ocean Eng. 2022;253: 111211.
24. Liu X, García MH. Three-dimensional numerical model with free water surface and mesh deformation for local sediment scour. J Waterw Port Coast Ocean Eng. 2008;134:203–17.
25. Gupta LK, Pandey M, Anand Raj P (2023) Numerical simulation of local scour around the pier with and without airfoil collar (AFC) using FLOW-3D. Environ Fluid Mech 1–19
26. Fuhrman DR, Baykal C, Sumer BM, Jacobsen NG, Fredsøe J. Numerical simulation of wave-induced scour and backfilling processes beneath submarine pipelines. Coast Eng. 2014;94:10–22.
27. Baykal C, Sumer BM, Fuhrman DR, Jacobsen NG, Fredsøe J. Numerical investigation of flow and scour around a vertical circular cylinder. Philos Trans R Soc A Math Phys Eng Sci. 2015;373:20140104.
28. Nicholson JC (2011) Design of wind turbine tower and foundation systems: optimization approach. https://doi.org/10.17077/etd.bhnu76gr
29. Whitehouse RJS, Harris JM, Mundon TR, Sutherland J (2010) Scour at offshore structures. In: Scour erosion, pp 11–20
30. Hirt CW, Nichols BD. Volume of fluid (VOF) method for the dynamics of free boundaries. J Comput Phys. 1981. https://doi.org/10.1016/0021-9991(81)90145-5.
31. Yakhot V, Orszag SA. Renormalization group analysis of turbulence. I.Basic theory. J Sci Comput. 1986;1:3–51.
32. Markatos NC. The mathematical modelling of turbulent flows. Appl Math Model. 1986;10:190–220.
33. Hwang RR, Jaw S-Y. Numerical prediction of turbulent wakes behind a square cylinder. J Mech. 1998;14:23–9.
34. Mastbergen DR, Van Den Berg JH. Breaching in fine sands and the generation of sustained turbidity currents in submarine canyons. Sedimentology. 2003;50:625–37.
35. Soulsby RL. Dynamics of marine sands: a manual for practical applications. Oceanogr Lit Rev. 1997;9:947.
36. Burnham J (2011) Modeling dams with computational fluid dynamics: past success and new directions. In: Association of state dam safety officials annual conference, pp 855–893
37. Aksoy AO, Eski OY. Experimental investigation of local scour around circular bridge piers under steady state flow conditions. J South Afr Inst Civ Eng. 2016;58:21–7.
38. Wei G, Brethour J, Grünzner M, Burnham J. The sedimentation scour model in FLOW-3D®. Flow Sci Rep. 2014;3:1–29.
39. Hu R, Wang X, Liu H, Chen D. Numerical study of local scour around tripod foundation in random waves. J Mar Sci Eng. 2022;10:475.
40. Zhao F, Yang M, Tang Y, Xu S Numerical simulation of offshore wind power pile foundation scour with different arrangements of artificial reefs. Front Mar Sci 10:1178370